Atmospheric
Chemistry
and Physics
Discussions

Open Access

The impact of polar stratospheric ozone loss on Southern Hemisphere stratospheric circulation and climate

J. Keeble[1], P. Braesicke[2], N. L. Abraham[3], H. K. Roscoe[4], and J. A. Pyle[3]

[1]University of Cambridge, Chemistry Department, Cambridge, UK
[2]Karlsruhe Institute of Technology, Institute for Meteorology and Climate Research, Karlsruhe, Germany
[3]NCAS/University of Cambridge, Chemistry Department, Cambridge, UK
[4]British Antarctic Survey, NERC, Cambridge, UK

Correspondence to: J. Keeble (jmk64@cam.ac.uk)

Discussion Paper | Discussion Paper | Discussion Paper | Discussion Paper |

ACPD

14, 18049–18082, 2014

The impact of polar stratospheric ozone loss

J. Keeble et al.

Title Page

Abstract | Introduction

Conclusions | References

Tables | Figures

|◀ | ▶|

◀ | ▶

Back | Close

Full Screen / Esc

Printer-friendly Version

Interactive Discussion

Title Page

Abstract | Introduction

Conclusions | References

Tables | Figures

|◄ | ►|

◄ | ►

Back | Close

Full Screen / Esc

Printer-friendly Version

Interactive Discussion

Abstract

The impact of polar stratospheric ozone loss resulting from chlorine activation on polar stratospheric clouds is examined using a pair of model integrations run with the fully coupled chemistry climate model UM-UKCA. Suppressing chlorine activation through heterogeneous reactions is found to produce modelled ozone differences consistent with observed ozone differences between the present and pre-ozone hole period. Statistically significant high latitude Southern Hemisphere (SH) ozone loss begins in August and peaks in October-November, with $> 75\%$ of ozone destroyed at 50 hPa. Associated with this ozone destruction is a $> 12\,\mathrm{K}$ decrease of the lower polar stratospheric temperatures and an increase of $> 6\,\mathrm{K}$ in the upper stratosphere. The heating components of this temperature change are diagnosed and it is found that the temperature dipole is the result of decreased shortwave heating in the lower stratosphere and increased dynamical heating in the upper stratosphere. The cooling of the polar lower stratosphere leads, through thermal wind balance, to an acceleration of the polar vortex and delays its breakdown by ~ 2 weeks. A link between lower stratospheric zonal wind speed, the vertical component of the EP flux, F_z, and the residual mean vertical circulation, $\overline{w}^*$, is identified. In December and January, increased westerly winds lead to increases in F_z, associated with an increase in tropopause height. The resulting increase in wavebreaking leads to enhanced downwelling/reduced upwelling over the polar cap. Many of the stratospheric signals modelled in this study propagate down to the troposphere, and lead to significant surface changes in December.

1 Introduction

The annually recurring Antarctic ozone hole is one of the most conspicuous examples of mankind's impact on the Earth system, and as such has received a great deal of scientific study. It is now well established that spring time chemical ozone loss in the polar lower stratosphere is the result of a combination of two processes: stable vortex

conditions, which lead to very low temperatures within the vortex and enable the formation of polar stratospheric clouds (PSCs), and increased anthropogenic emissions of ozone depleting substances (ODS) (WMO, 2011). More recently it has also become apparent that the ozone hole has had significant impacts on stratospheric temperatures, atmospheric circulation and surface climate.

Since the discovery of the Antarctic ozone hole in the mid-1980s (Farman et al., 1985) rapid advances in the understanding of the causes of high latitude stratospheric ozone depletion have taken place. The large Southern Hemisphere (SH) spring time ozone losses documented since the mid-1980s result from increased emissions of anthropogenic chlorofluorocarbons (CFCs) combined with unique meteorological conditions at high southern latitudes. Throughout the latter half of the 20th century, the use and emission of CFCs led to a large increase in the total amount of chlorine in the stratosphere (WMO, 2011). The effects of this increased chlorine loading have been small on a global scale, leading to a global average depletion of 3–4 % of the total ozone column. However, over Antarctica, due to heterogeneous chemistry occurring on PSCs the depletion is much more severe, with vortex averaged total ozone column in October 40 % below 1980 values (WMO, 2011).

For typical stratospheric mixing ratios of HNO_3 and H_2O, PSC particles form when temperatures fall below 195 K, which is the case for much of the winter over Antarctica. PSCs lead to large decreases in high latitude, lower stratospheric ozone mixing ratios through two processes. Firstly, these particles act as surfaces where chlorine activation can occur, converting the chlorine reservoir species HCl and $ClONO_2$ into Cl_2 (e.g. Solomon et al., 1986). Cl_2 photolysis exists throughout winter in the vortex edge region (e.g. Schoeberl et al., 1992; Lee et al., 2001), but only occurs in the vortex core when sunlight returns in spring, and the resulting chlorine radicals destroy ozone through catalytic cycles (e.g. Molina and Molina, 1987). Secondly, as the particles sediment out, they deplete NO_y in the lower stratosphere (Toon et al., 1986). This process of denitrification prevents the reformation of the reservoir species until the collapse of the polar vortex, prolonging the period of ozone destruction. The development of a strong,

stable vortex around Antarctica during SH winter and spring isolates air over the pole and prevents mixing between high and mid latitude air masses (e.g. Tuck, 1989; Schoeberl and Hartmann, 1991; Waugh and Polvani, 2010) which allows for very high levels of chemical ozone depletion. The arctic vortex is not as stable as that of the Antarctic due to increased planetary wave activity in the Northern Hemisphere (NH). This limits the volume of air in which PSCs can form, and the amount of time over which they persist, preventing regular large scale NH ozone loss. As such, this study focuses on the impact of stratospheric ozone depletion on SH climate and circulation. For a full review of stratospheric ozone depletion, see Solomon (1999) and references therein.

Coincident with the development of the annually recurring ozone hole have been significant changes to SH climate. Analysis of radiosonde measurements (Thompson and Solomon, 2002) has shown that from 1970 to 2000 the SH spring time lower stratosphere cooled significantly, reaching a maximum cooling of 6–10 K in November. This cooling persists through SH summer and autumn, although with a reduced magnitude (1–2 K), with no statistically significant trend observed during SH winter. While the lower stratosphere has cooled, during SH spring statistically significant warming is observed at 30 hPa. It should be noted that the trends presented in Thompson and Solomon (2002) are averaged over a number of radiosonde stations, most of which are north of 70° S. Roscoe et al. (2003) present an analysis for measurements made at Halley, the southernmost station, and determine a maximum cooling of 10–18 K in November, indicating cooling in the core of the vortex is greater than that presented by Thompson and Solomon.

While analysis of observational data suggests a link between polar ozone depletion and Antarctic climate change, due to changes in other aspects of the atmospheric system, most notably greenhouse gas concentrations, observations alone cannot prove causality. Therefore, a number of idealised model studies have attempted to determine the impact of stratospheric ozone loss by separating the effects of ozone depletion and global warming (Gillett and Thompson, 2003; Arblaster and Meehl, 2006; Braesicke et al., 2006; Garcia and Randel, 2008; Perlwitz et al., 2008; Waugh et al.,

Title Page

Abstract | Introduction

Conclusions | References

Tables | Figures

|◄ | ►|

◄ | ►

Back | Close

Full Screen / Esc

Printer-friendly Version

Interactive Discussion

2009; McLandress et al., 2010; Son et al., 2010; Polvani at al., 2011; Orr et al., 2012a). While the majority of studies have focused on the stratospheric and tropospheric response to ozone depletion, several authors have explored the impacts on the Southern Ocean (Sigmond and Fyfe, 2010; Sigmond et al., 2011). In order to assess the impacts of Antarctic ozone depletion on climate these studies have either used prescribed ozone climatologies, or varied either GHGs or ODSs while keeping the other fixed. Both of these methods come with caveats. Using prescribed ozone fields prevents chemistry–climate feedbacks from developing within the model, which are known to be important for a full understanding of the impacts of ozone depletion. Varying ODS allows chemistry–climate interactions, but affects gas phase chemistry throughout the stratosphere and also changes the concentration of GHGs between the simulations, as CFCs have very high global warming potentials (WMO, 2011).

In this paper we present a method for assessing the climatic impact of polar stratospheric ozone loss by supressing chlorine activation through reactions occurring on the surface of PSC particles. Using this method we determine the modelled change in ozone that occurs over Antarctica as a consequence of heterogeneous chemistry, and the subsequent impact on SH climate and stratospheric circulation. This has the advantage of leaving the integrations identical except for the simulation of polar stratospheric ozone loss at high latitudes. It allows the modelled ozone distribution to remain consistent with the flow field and for chemistry–climate and dynamical feedbacks to occur, which are particularly important due to the radiative impact of ozone. We do not suggest that this method is better than that used in other studies, but highlight the suitability of this method for studying chemistry–climate interactions in a chemistry climate model.

Here we present results of a modelling study assessing the impact of high latitude polar ozone loss on SH climate and stratospheric circulation. In Sect. 2 the chemistry climate model used for this study is discussed, focussing on its handling of heterogeneous chemical processes, and the simulations are outlined. In Sect. 3 we present the impact of chlorine activation on polar ozone, and the effect polar stratospheric ozone

depletion has on temperature, zonal winds, geopotential height and downwelling over the polar cap. In Sect. 4 we present a detailed discussion of the physical mechanisms responsible for the changes shown in Sect. 3. Finally we examine the coupling of the stratosphere and troposphere by quantifying the impact of stratospheric ozone loss on surface climate in Sect. 5.

2 Description of model and simulations

In order to determine the impact of lower stratospheric ozone loss on SH climate and global circulation we use version 7.3 of the Met Office's Unified Model HadGEM 3-A configuration (Hewitt et al., 2011) coupled with the United Kingdom Chemistry and Aerosol module (hereafter referred to as UM-UKCA). The model is run using an updated version of the stratospheric chemistry configuration of UM-UKCA described in Morgenstern et al. (2009), at a horizontal resolution of 2.5° latitude by 3.75° longitude, with 60 vertical levels and a model top at ~ 84 km.

For this study, two simulations are considered, named REF2000 and NHC. REF2000 is a thirty year time-slice integration run with perpetual year 2000 boundary conditions, including sea surface temperatures, sea ice extent, greenhouse gas, CFC and aerosol loadings. NHC is identical to REF2000 except that chlorine activation due to heterogeneous reactions on PSC particles is suppressed, preventing large spring time ozone losses in the lower polar stratosphere. In both integrations gas phase ozone loss is treated in the same manner and the total Cl_y loading is the same. The difference lies in the treatment of the modelled PSCs. While both integrations were run for 30 years, the first ten years are discarded as spin up time for the model, and climatologies presented here comprise the last 20 years of the model run.

In UM-UKCA, two types of PSC particles are modelled: nitric acid trihydrate (NAT) and mixed NAT/ice polar stratospheric clouds, calculated following Chipperfield (1999) assuming thermodynamic equilibrium with gas-phase HNO_3 and H_2O. PSC particles form in both model integrations and therefore the radiative impacts of the clouds

themselves will not change between the two runs, but for any chemistry–climate feedbacks. In REF2000, five heterogeneous reactions occur on PSC particles, activating the chlorine within the reservoir species. These reactions are:

$$\text{ClONO}_2 + \text{H}_2\text{O} \quad \rightarrow \quad \text{HOCl} + \text{HNO}_3 \tag{R1}$$
$$\text{ClONO}_2 + \text{HCl} \quad \rightarrow \quad 2\text{Cl} + \text{HNO}_3 \tag{R2}$$
$$\text{HOCl} + \text{HCl} \quad \rightarrow \quad 2\text{Cl} + \text{H}_2\text{O} \tag{R3}$$
$$\text{N}_2\text{O}_5 + \text{H}_2\text{O} \quad \rightarrow \quad 2\text{HNO}_3 \tag{R4}$$
$$\text{N}_2\text{O}_5 + \text{HCl} \quad \rightarrow \quad \text{Cl} + \text{NO}_2 + \text{HNO}_3 \tag{R5}$$
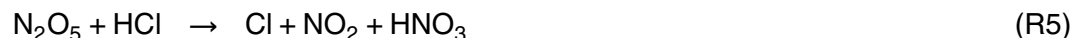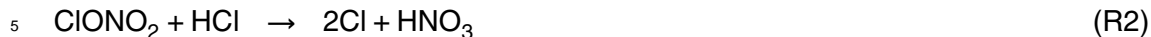
In the NHC simulation, modelled PSC particles are treated as inert in terms of their chemistry. This is achieved by setting the surface area density of type I and II PSC particles to $0\,\text{cm}^2\,\text{cm}^{-3}$ when calculating the rates of the 5 heterogeneous reactions listed above. This method is similar to that employed by Karpechko et al. (2013), who prevent PSC formation by fixing the air temperature passed to their heterogeneous chemistry module to 200 K. However, as we allow PSCs to form, we are able to capture the radiative impacts of the clouds themselves, which trap outgoing longwave radiation (Sloan and Pollard, 1998). The treatment of liquid sulphate aerosols remains identical in both simulations: aerosol background levels are prescribed in both simulations using a perpetual year 2000 aerosol surface area density updated from SPARC (2006), as described by Eyring et al. (2008).

The result of this method is to produce two integrations which differ predominantly in the mixing ratios of ozone in the lower stratosphere at high latitudes. This ozone difference then acts as a driver for any subsequent chemical and/or climatological differences between the two integrations. Chlorine activation through heterogeneous chemistry and the subsequent ozone catalytic loss cycles are nonlinear processes and a threshold value of stratospheric total inorganic chlorine (Cl_y) must be reached for these processes to lead to large ozone depletion. Manzini et al. (2003) estimate this

threshold value to be ~ 2.2 ppbv. Given this, we argue that suppressing chlorine activation on PSCs is, to first order, comparable to running the simulation with 1960s levels of stratospheric Cl_y from the point of view of studying Antarctic polar stratospheric ozone loss. We allow the modelled ozone field to respond to changing dynamics and remain consistent with the modelled flow field, unlike experiments in which ozone is prescribed. In this way we preserve chemistry–climate feedbacks between the two runs to fully understand the effects of stratospheric ozone depletion on both climate and circulation.

3 Stratospheric response to chlorine activation on PSCs

Results in this study are presented as differences between the monthly mean climatologies of the two simulations. The difference is calculated as REF2000 – NHC so as to highlight the impact of ozone depletion. Stippling denotes significance at the 95 % confidence level using a two-tailed Student's t test.

3.1 Ozone

The percentage change in monthly, zonal mean ozone between the two integrations, averaged over the polar cap (90–75° S) is shown in Fig. 1. Modelled ozone loss begins in August at approximately 30 hPa and descends in altitude through time, with more than 75 % of ozone destroyed during late October and November at 50 hPa. Ozone concentrations in the lower stratosphere remain reduced throughout the summer and autumn. From December to March there is a statistically significant increase in ozone mixing ratios at 20 hPa. Tropospheric ozone mixing ratios are greatly reduced throughout the year due to a decrease in STE. However, the version of the model used here does not have a comprehensive tropospheric chemistry scheme and therefore tropospheric ozone changes are not considered in this analysis. For a discussion on the impact of stratospheric ozone changes on STE in UM-UKCA see Morgenstern et al. (2013) and Braesicke et al. (2013).

The timing and vertical extent of the ozone loss is comparable with observed changes in ozone mixing ratios between pre-ozone hole and ozone hole eras (Thompson et al., 2011). However, the maximum modelled ozone loss in late spring is not as great as is observed, where $> 90\%$ loss is seen at 70 hPa. This is for two reasons:
firstly, there is no increased loss due to gas phase chemistry as the total chlorine burden of the atmosphere is constant between the two simulations. Secondly, the stratospheric chemistry scheme in this version of the model does not include heterogeneous reactions involving bromine, the inclusion of which would to lead to increased ozone depletion, especially when combined in bromine-chlorine cross reactions (e.g. McElroy
et al., 1986). It should be noted that the observed composite difference presented in Thompson et al. (2011) extends up to 30 hPa, and so does not capture the region of increased summer ozone mixing ratios modelled here.

The effects of heterogeneous chemistry on ozone extend beyond the polar vortex. Figure 2 shows the change in global, monthly mean, zonal mean total column ozone
between the two simulations, in Dobson Units. While the largest ozone decreases are found in the SH spring time polar vortex, total column ozone over the entire southern hemisphere has decreased, with decreases of more than 15DU at the equator. These decreases are statistically significant at the 95 % confidence level at almost all latitudes. The NH response is more complicated: while column ozone is significantly
depleted within the spring time polar vortex, throughout late autumn and winter there is a statistically significant increase in column ozone of 20–30 DU at $\sim 60°$ N. This is a noteworthy feature, as the difference in the chemistry between the two integrations (i.e. the activation of chlorine through heterogeneous reactions) can only lead to ozone destruction and should predominantly affect the SH, where PSCs are more abundant.
Increased winter column ozone indicates a dynamical response, with increased poleward and downward transport of ozone, suggesting changes to the Brewer–Dobson Circulation (BDC; after Brewer, 1949; Dobson, 1956). If this is a robust response to increased NH polar ozone loss, it could be used as an early indicator for NH transport changes. It should be stressed that the effects beyond the vortex are the result of

the model reaching a new equilibrium state and have been accumulated over previous years, and that heterogeneous processes within the vortex do not lead to mid latitude ozone loss in the same month.

3.2 Temperature, zonal wind, geopotential height and vertical circulation changes

Figure 3 shows the monthly, zonal mean temperature difference between the two integrations averaged over 90–75° S, plotted as a function of altitude and month. Modelled polar ozone loss leads to a strongly seasonal response. Cooling of the lower polar stratosphere begins in September when sunlight returns to the core of the polar vortex, and continues through until March. Maximum cooling occurs from November to December, during which time temperatures at 70 hPa decrease by 12 K. Strong cooling of the polar lower stratosphere resulting from ozone loss is consistent with observations (Thompson and Solomon, 2002; Roscoe et al., 2003) and idealised model studies (Gillett and Thompson, 2003; Manzini et al., 2003; Karpechko et al., 2010). There is no statistically significant change in temperature during the summer, in agreement with observations. While ozone loss causes the lower stratosphere to cool, the upper stratosphere warms, beginning in October and persisting through to January–February. Maximum warming occurs in December, when polar cap averaged temperatures increase by > 6 K at 10 hPa. The results presented by Thompson and Solomon (2002) extend up to 30 hPa, and therefore do not show the region of upper stratospheric warming modelled in this study. However, warming of the upper stratosphere is in agreement observations presented by Young et al. (2013), and with a number of modelling studies which assess the impact of ozone loss above 30 hPa (e.g. Shindell and Schmidt, 2004).

Figure 4 shows the impact of modelled polar ozone loss on the zonal mean zonal wind, averaged over 50—70° S. The temperature change due to polar ozone loss leads to a statistically significant acceleration of the modelled westerlies around Antarctica from mid spring to late summer, and also causes the polar vortex to shift polewards. As with the temperature response, the zonal wind changes are highly seasonal, with

no statistically significant changes during autumn and summer. As well as accelerating the polar vortex, the cooling due to polar ozone loss also causes the breakdown of the polar vortex to be delayed by approximately 2 weeks. For any given month, a delay in the transition from westerlies to easterlies is realised as an increase in the height of the zero wind line, highlighted in bold in Fig. 4 for the REF2000 integration. A delayed breakup of the polar vortex resulting from increased ozone loss is in good agreement with other studies (Waugh et al., 1999; Haigh and Roscoe, 2009; Karpechko et al., 2010; McLandress et al. 2010). The changes to zonal wind speed are not confined to the stratosphere, with a nonsignificant increase in westerly wind descending into the troposphere in December. The extension of the zonal wind response into the tropo-sphere is also noted by other authors (e.g. Polvani et al., 2011).

Figure 5 shows the difference in geopotential height between the two integrations, averaged from 90–75° S. Large negative changes of more than 200 m are modelled throughout the depth of the stratosphere from October to January, with statistically sig-nificant changes persisting through to March. The largest deceases occur in the lower stratosphere in November and December, during which geopotential height decreases of > 500 m are modelled. These changes are indicative of a stronger, colder polar vor-tex. Further to the stratospheric changes, decreased geopotential height anomalies are modelled to propagate down into the troposphere, highlighted in Fig. 5 by the 10 m contour intervals as the changes are not on the same order as those in the strato-sphere. The geopotential height changes modelled here are in good agreement with other model studies (e.g. Gillett and Thompson, 2003) and observations (Thompson and Solomon, 2002).

Differences to the mean residual vertical circulation, $\overline{w}^*$, averaged over the polar cap (90–75° S) are shown in Fig. 6, with negative changes indicating increased down-welling/reduced upwelling. Downwelling over the polar cap is increased from late spring to early summer, with statistically significant changes in November and December throughout the depth of the stratosphere. Increased downwelling at high southern lat-itudes has been noted in other model studies (e.g. Manzini et al., 2003; McLandress

et al., 2010). The changes to the mean residual vertical velocity are strongly seasonal, and occur at the time modelled stratospheric circulation over the polar cap changes from downwelling to upwelling.

4 Physical mechanisms in the stratosphere

In order to further investigate the stratospheric temperature differences between the two simulations we calculate the dynamical and short wave heating components of the temperature response to polar ozone loss. Short wave heating rates are diagnosed directly from the model, and the difference between the two integrations is shown in Fig. 7a. In the lower stratosphere, shortwave heating rates decrease during Austral spring and summer, with a maximum reduction of $> 0.6\,\mathrm{K\,day^{-1}}$ in November–December. The decrease in shortwave heating is coincident with the region of depleted ozone, and this is likely the dominant control, although changes to other radiatively important trace gases will play a role. Shortwave heating increases in November at 10 hPa, and this increase persists through time until late summer, descending in altitude during this period. This is coincident with an increase in ozone mixing ratios.

Dynamical heating is not directly diagnosed by the model, and is calculated using the ageostrophic equation from Dunkerton et al. (1981):

$$\overline{Q}_d^{\theta} = -\rho_0^{-1} \left\{ \rho_0 \left[\left(\frac{\overline{\theta}_{\varphi}}{a\overline{\theta}_z} \right) \overline{v'\theta'} + \overline{w'\theta'} \right] \right\}_z - \frac{1}{a}\,\overline{\theta}_{\varphi}\overline{v}^* - \overline{\theta}_z\overline{w}^* \tag{1}$$

where $\overline{Q}_d^{\theta}$ is the dynamical heating rate of the zonally averaged potential temperature, θ is the potential temperature, ρ_0 is the background density, subscripts φ and z denote the partial derivatives with respect to latitude and height respectively, a is the radius of the Earth (6371 km), v and w are the meridional and vertical wind components respectively and $\overline{v}^*$ and $\overline{w}^*$ are the meridional and vertical components of the mean

residual circulation respectively. In order to compare with the short wave heating rates from the model, the result is then converted into absolute temperature using:

$$\overline{Q}_d = \overline{Q}_d^{\,\theta} \left(\frac{p}{p_0} \right)^{R/C_p} \tag{2}$$

where p is pressure, p_0 is surface pressure (assumed to be 1000 hPa), R is the gas

5 constant of air and C_p is the specific heat capacity. Figure 7b shows the polar cap average difference in dynamical heating between the two simulations. There is a strong increase in dynamical heating during late spring and summer, extending throughout the depth of the stratosphere.

The dipole in the temperature response to ozone loss can therefore be explained by

10 a combination of changes to shortwave and dynamical heating. Decreased ozone mixing ratios lead to pronounced cooling of the lower stratosphere. This is to some extent mitigated by a small increase in dynamical heating below 10 hPa. The peak increase in temperature in the middle stratosphere is the result of an increase to both shortwave and dynamical heating. Above 10 hPa there is little change to shortwave heating, and

15 the increase in temperatures is almost solely due to increases in dynamical heating, consistent with large changes to $\overline{w}^*$ at these altitudes, but little change to ozone.

Changes to stratospheric temperatures lead to changes in longwave heating rates. As we use time averaged data for this study it is not straightforward to fully close the heat budget, and so we do not explore these changes in any great detail. However,

20 the strong cooling of the lower stratosphere leads to decreased emission of downward longwave radiation, consistent with Grise et al. (2009). Averaged over the polar cap, this leads to a weak, non-significant cooling propagating down into the troposphere during December (Fig. 3). Tropospheric changes are explored further in Sect. 5. Cooling of the lower stratosphere increases the midlatitude to pole temperature gradient, which

25 drives the increased zonal wind speeds shown in Fig. 4 through thermal wind balance and also causes the polar vortex to shift poleward.

Changes to the mean residual vertical velocity (shown in Fig. 6) are a measure of changes to the BDC. Differences in Eliassen–Palm (EP) Flux divergence between the two integrations, averaged over 50–70° S, are shown in the upper panel of Fig. 8. Negative values represent decreased flux divergence, i.e. increased convergence, and indicate increased wave breaking. During mid to late spring there is a weak decrease in wave breaking, a result which is consistent with McLandress et al. (2010). The spring time decrease in EP flux divergence has received little study, and the mechanisms controlling it are poorly understood. From late spring to late summer wave breaking increases, starting in November at ∼ 1 hPa and persisting through to February, decreasing in altitude with time. Increased wave breaking in the mid to high latitudes during summer drives increased downwelling over the polar cap (Fig. 6). Using Fourier transform analysis (not shown here) we are able to determine that it is predominantly resolved planetary waves which drive these changes, which is in agreement with other authors (e.g. McLandress et al., 2010).

It is important to determine whether the changes to wave breaking are the result of changes to the wave activity entering the stratosphere or to alterations to the propagation of waves through the stratosphere. The 100 hPa vertical component of the EP Flux, which is proportional to the meridional heat flux ($\overline{v'T'}$), can be used as a measure of upward propagating planetary wave activity entering the stratosphere from the troposphere. The lower panel of Fig. 8 shows the difference in the 100 hPa vertical EP Flux vector, F_z, between the two simulations, averaged over 50–70° S, in red. During the spring there is a weak decrease in F_z in the mid to high latitudes, while in the summer there is a strong increase over a similar latitude range. These changes coincide with the decrease/increase in wave breaking in the spring/summer modelled in the lower stratosphere, and are statistically significant in December and January. However, although F_z, and therefore wave driving, show slight decreases in October and November, wave breaking at ∼ 1 hPa in November has increased. Also, large increases in F_z are modelled in June, with no significant change to EP-flux divergence at that time, while the decrease in wave propagation in September–October is near zero but wave breaking

is greatly reduced. Therefore, changes to wave propagation from the troposphere to the stratosphere are not likely the dominant control on the changes to wave breaking resulting, although likely do play a role in the increased wave breaking modelled in December-January.

Also shown in the lower panel of Fig. 8 are changes to tropopause height averaged over 50–70° S, in blue. The largest tropopause height changes (> 125 m) are modelled from November to January, and result from the cooling of the lower stratosphere due to ozone depletion and the resultant changes to the lapse rate. The summer time tropopause height changes occur together with the large increases to F_z in December–January, and suggest a relationship between the two, although the tropopause height response leads the changes to F_z by a month. As we compare two different equilibrium states it is difficult here to identify a causal link between changes to tropopause height and F_z. However, the two metrics respond in a consistent way, suggesting a relationship between tropopause height and the wave driving entering the stratosphere from the troposphere. For a more detailed discussion on the impacts of ozone depletion on tropopause height changes see Braesicke et al. (2013).

If changes to the wave driving propagating from the troposphere to the stratosphere play only a minor role in the changes to wave breaking, polar ozone loss must lead to alterations in how planetary waves are able to propagate through the stratosphere. Vertical planetary wave propagation is only possible through westerly winds, and is reduced when zonal wind speeds exceed a critical value, U_c, such that a propagation window exists when the following condition is satisfied:

$$0 < u < U_c \tag{3}$$

The increases in zonal wind speed in austral spring limit planetary wave propagation through the stratosphere by increasing westerly winds above the threshold U_c. Conversely, the increase in height of the zero wind line and the delayed break down of the polar vortex, discussed above, allow planetary waves to propagate higher into the stratosphere and over a longer period of time in the summer. This is shown in Fig. 8,

Title Page

Abstract | Introduction

Conclusions | References

Tables | Figures

|◄ | ►|

◄ | ►

Back | Close

Full Screen / Esc

Printer-friendly Version

Interactive Discussion

where decreased EP flux divergence occurs around the time of the descent of the zero wind line. This, combined with the changes to F_z discussed above, results in statistically significant increases in wave breaking in the mid to high latitudes in December and January.

The link between changes to zonal wind speed, vertical planetary wave propagation and downwelling can be explored further by analysing latitude time sections at a set altitude in the lower stratosphere, as shown for 70 hPa in Fig. 9. From September to November there is a weak negative correlation between zonal wind speed (Fig. 9 upper panel) and the vertical component of the EP Flux vector (Fig. 9 lower panel). This is consistent with zonal wind speeds increasing above the critical value U_c, preventing some planetary waves from propagating higher into the stratosphere. As planetary wave breaking deposits easterly momentum, the decrease in planetary wave propagation helps to strengthen the polar vortex. In this way a positive feedback is set up in spring such that increased westerlies lead to increased filtering of planetary waves, which results in decreased wave breaking and deposition of easterly momentum, preventing the deceleration of the polar jet and causing it to persist for longer (consistent with the mechanism proposed by Orr et al., 2012a). However, the meridional heat flux and $\overline{w}^*$ differences are not significant at the 95 % confidence level, and it is difficult to infer a causal relationship.

In summer, a much more robust relationship is evident. From November to January westerly wind speeds at 60–80° S are greatly increased at 70 hPa due to thermal wind balance and the delay of the breakup of the vortex, as discussed above. During December and January, across the same latitude range, the vertical propagation of planetary waves through this layer is enhanced. Increased propagation through the layer leads to increased wave breaking above, driving increased downwelling at 70 hPa, shown by changes to $\overline{w}^*$ (Fig. 9, lower panel). While the increased downwelling through the 70 hPa layer occurs at the same time as the enhanced meridional heat flux, it does not occur at the same latitude range, unlike the changes in zonal wind speed and meridional heat flux. Instead it is displaced poleward of the region of enhanced vertical

planetary wave propagation. In this stage of the vortex lifetime a negative feedback now operates between zonal wind speed and planetary wave propagation. Increased westerlies allow increased wave breaking, which results in the increase of deposition of easterly momentum, decelerating the vortex and ultimately causing it to collapse. This relationship also holds for regions where westerly wind speed decreases. In December, as the polar jet moves poleward, there is a decrease in westerly wind speed at 45–30° S, which correlates to a region of decreased vertical planetary wave propagation, and a decrease in downwelling.

5 Tropospheric changes and surface impacts

As discussed in the previous sections, the temperature, zonal wind and geopotential height differences resulting from stratospheric ozone loss extend down into the troposphere, reaching the modelled surface in December. Figure 10 shows the impact of increased stratospheric ozone loss on December pressure and temperature at 16 km (in the lower stratosphere, $\sim 100\,$hPa), 8.5 km (at the tropopause, $\sim 250\,$hPa) and the surface ($\sim 1000\,$hPa). Statistically significant temperature decreases extend downwards from the lower stratosphere to the surface of the model. At 16 km the cooling, as much as 10 K in the core of the vortex, is strongly zonally symmetric, as is the cooling at 8.5 km, although the magnitude is decreased. Associated with this is an increase in tropopause height by 300–500 m, resulting from a decrease in lower stratospheric temperatures and changes to the lapse rate (explored further in Braesicke et al., 2013). While the temperature response in the lower stratosphere and free troposphere is zonally symmetric, the surface temperature response shows a marked asymmetry. Most of the Antarctic continent cools by more than 0.5 °C, with statistically significant cooling of more than 1 °C over the Ross Ice Shelf and much of East Antarctica. Conversely the Antarctic Peninsula warms by more than 0.5 °C. As the version of the model used in this study uses prescribed sea surface temperatures and sea ice, it is likely to damp the surface response. Despite this caveat, the asymmetric modelled surface response is

in good agreement with observations (Thompson and Solomon, 2002) and numerous model studies (e.g. Gillett and Thompson, 2003).

Modelled ozone losses lead to a zonally symmetric reduction in pressure in the lower stratosphere, extending down from 16 km to the surface. Surface pressure decreases over the Antarctic continent, and increases north of 65° S. This pattern closely resembles the positive phase of the Southern Annular Mode (SAM), and is in good agreement with other modelling studies. The surface response extends far beyond the Antarctic continent, and it is well known that the SAM influences SH storm tracks, precipitation and near surface winds over a large area of the Southern Hemisphere (e.g. Thompson et al., 2011).

6   Summary and conclusions

We have presented results from an idealised model study using UM-UKCA to assess the impacts of lower stratospheric ozone loss on SH stratospheric circulation and climate. Two simulations were run, both using perpetual year 2000 boundary conditions. The first used a full stratospheric chemistry scheme, while in the second heterogeneous chemistry occurring on PSCs was suppressed. This resulted in two simulations, one of which models severe, high latitude, spring time ozone depletion and one which does not. In this way we quantify the effects of polar stratospheric ozone depletion on four key variables: temperature, zonal wind speed, geopotential height and polar downwelling. The method used in this study differs from those used in previous studies on the climatic impacts of ozone depletion and is well suited to studying the feedbacks of chemistry–climate and chemical–dynamical interactions in an idealised sense.

Through heterogeneous reactions occurring on the surfaces of PSCs chlorine held within the reservoir species HCl and $ClONO_2$ is converted into reactive species which deplete ozone through catalytic cycles when sunlight returns to the polar vortex in spring. The increased active chlorine causes lower stratospheric ozone to be depleted by more than 50 % from September to January, with peak depletion of 75 % from

October to November. While this is in good agreement with observations and other modelling studies, we also model an increase in ozone mixing ratios between 30–10 hPa from December to March due to changes in stratospheric dynamics. Despite also being modelled in other studies, this feature is not commonly included in studies using prescribed ozone fields as it lies above the top level of radiosonde measurements. However, due to the radiative impact of ozone, it is an important feature for understanding chemistry–climate interactions and feedbacks. Ozone changes extend beyond the spring time polar vortex. Despite global Cl_y being constant between the two runs, zonal mean total column ozone is reduced at almost all latitudes, with equatorial total column ozone reduced by 15DU. However, column ozone at 60° N is increased by up to 30 DU throughout late spring and winter due to increased northward transport of ozone by a faster BDC. If this feature is shown to be a consistent response to NH polar ozone depletion, changes to total column ozone trends at this latitude may provide early evidence for changing levels of NH ozone depletion or the strength of the BDC in general. Further work is required to determine the effects of Arctic stratospheric ozone depletion on NH total column ozone trends.

Polar ozone depletion produces a vertical dipole in the temperature response: while the lower stratosphere cools due to decreased shortwave heating, the middle and upper stratosphere warm due to a combination of dynamical heating (the dominant component) and increased shortwave heating at ~ 10 hPa. Increased dynamical heating below 10 hPa somewhat mitigates the shortwave cooling of the lower stratosphere (consistent with Orr et al., 2012b). The cooling of the lower polar stratosphere increases the midlatitude to pole temperature gradient, causing an acceleration and poleward shift of the polar vortex, and delaying the breakup of the polar vortex. We demonstrate a relationship between zonal wind speed, upward propagating planetary wave activity as diagnosed by the vertical component of the EP flux vector, and mean residual vertical velocity. In spring increased zonal mean wind speeds limit vertical planetary wave propagation, inducing a positive feedback which strengthens further the polar vortex due to the decreased deposition of easterly momentum resulting from wave breaking.

Conversely, in summer increased zonal wind speeds and the delayed breakup of the polar vortex allows planetary wave activity to propagate higher into the stratosphere for a longer period of time. This results in increased wave breaking, as diagnosed by increased EP flux divergence, which drives increased downwelling over the pole throughout November and December. Our analysis indicates that changes to wave propagation from the troposphere to the stratosphere plays only a minor role in the changes to wave breaking resulting from polar ozone depletion. The change in wave propagation is coincident with an increase in tropopause height in December and January, although there is no change in F_z despite increased tropopause height in June.

Lower stratospheric ozone depletion also drives statistically significant tropospheric changes which extend down to the surface. In December, stratospheric ozone depletion causes surface pressure to decrease poleward of $\sim 60°$ S, and increase from 60–30° S in a pattern resembling the positive phase of the SAM. Surface temperature is also affected, with significant cooling modelled over much of the Antarctic continent, and warming over the Antarctic Peninsula.

As ozone recovers over the 21st century, the changes discussed in this paper will likely reverse. It remains an important discussion as to how ozone recovery and global warming will offset one another or combine to produce rapid change.

References

Arblaster, J. M. and Meehl, G. A.: Contributions of external forcings to Southern Annular Mode trends, J. Clim., 19, 2896–2905, doi:10.1175/JCLI3774.1, 2006.

Braesicke, P., Hurwitz, M. M., and Pyle, J. A.: The stratospheric response to changes in ozone and carbon dioxide as modelled with a GCM including parameterised ozone chemistry, Meteorol. Z., 15, 343–354, doi:10.1127/0941-2948/2006/0124, 2006.

Braesicke, P., Keeble, J., Yang, X., Stiller, G., Kellmann, S., Abraham, N. L., Archibald, A., Telford, P., and Pyle, J. A.: Circulation anomalies in the Southern Hemisphere and ozone changes, Atmos. Chem. Phys., 13, 10677–10688, doi:10.5194/acp-13-10677-2013, 2013.

Brewer, A. W.: Evidence for a world circulation provided by the measurements of helium and water vapour distribution in the stratosphere, Q. J. Roy. Meteor. Soc., 75, 351–363, 1949.

Chipperfield, M. P.: Multiannual simulations with a three-dimensional chemical transport model, J. Geophys. Res., 104, 1781–1805, 1999.

Dobson, G. M. B.: Origin and distribution of the polyatomic molecules in the atmosphere, P. R. Soc. Lond. A, 236, 187–193, 1956.

Dunkerton, T., Hsu, C.-P. F., and McIntyre, M. E.: Some Eulerian and Lagrangian diagnostics for a model stratospheric warming, J. Atmos. Sci., 38, 819–843, 1981.

Eyring, V., Chipperfield, M. P., Giorgetta, M. A., Kinnison, D. E., Manzini, E., Matthes, K., Newman, P. A., Pawson, S., Shepherd, T. G., and Waugh, D. W.: Overview of the new CCM-Val reference and sensitivity simulations in support of upcoming ozone and climate assessments and the planned SPARC CCM-Val, SPARC Newsletter, 30, 20–26, 2008.

Farman, J. C., Gardiner, B. G., and Shanklin, J. D.: Large losses of total ozone in Antarctica reveal seasonal ClO_x/NO_x interaction, Nature, 315, 207–210, 1985.

Garcia, R. R. and Randel, W. J.: Acceleration of the Brewer–Dobson circulation due to increases in greenhouse gases, J. Atmos. Sci., 65, 2731–2739, doi:10.1175/2008JAS2712.1, 2008.

Gillett, N. P. and Thompson, D. W. J.: Simulation of recent Southern Hemisphere climate change, Science, 302, 273–275, doi:10.1126/science.1087440, 2003.

Grise, K. M., Thompson, D. W. J., and Forster, P. M.: On the role of radiative processes in stratosphere-troposphere coupling, J. Climate, 22, 4154–4161, doi:10.1175/2009JCLI2756.1, 2009.

Haigh, J. D. and Roscoe, H. K.: The final warming date of the Antarctic polar vortex and influences on its interannual variability, J. Climate, 22, 5809–5819, 2009.

Hewitt, H. T., Copsey, D., Culverwell, I. D., Harris, C. M., Hill, R. S. R., Keen, A. B., McLaren, A. J., and Hunke, E. C.: Design and implementation of the infrastructure of

The impact of polar stratospheric ozone loss

J. Keeble et al.

HadGEM3: the next-generation Met Office climate modelling system, Geosci. Model Dev., 4, 223–253, doi:10.5194/gmd-4-223-2011, 2011.

Karpechko, A. Y., Gillett, N. P., Gray, L. J., and Dall'Amico, M.: Influence of ozone recovery and greenhouse gas increases on Southern Hemisphere circulation, J. Geophys. Res., 115, D22117, doi:10.1029/2010JD014423, 2010.

Karpechko, A. Y., Backman, L., Thölix, L., Ialongo, I., Andersson, M., Fioletov, V., Heikkalä, A., Johnsen, B., Koskela, T., Kyrölä, E., Lakkala, K., Myhre, C. L., Rex, M., Sofieva, V. F., Tamminen, J., and Wohltmann, I.: The link between springtime total ozone and summer UV radiation in Northern Hemisphere extratropics, J. Geophys. Res.-Atmos., 118, 8649–8661, doi:10.1002/jgrd.50601, 2013.

Lee, A. M., Roscoe, H. K., Jones, A. E., Haynes, P. H., Shuckburgh, E. F., Morrey, M. J., and Pumphrey, H. C.: The impact of the mixing properties within the Antarctic stratospheric vortex on ozone loss in spring, J. Geophys. Res., 106, 3203–3211, 2001.

Manzini, E., Steil, B., Brühl, C., Giorgetta, M. A., and Krüger, K.: A new interactive chemistry–climate model: 2. Sensitivity of the middle atmosphere to ozone depletion and increase in greenhouse gases and implications for recent stratospheric cooling, J. Geophys. Res., 108, 4429, doi:10.1029/2002JD002977, 2003.

McElroy, M. B., Salawitch, R. J., Wofsy, S. C., and Logan, J. A.: Reductions of Antarctic ozone due to synergistic interactions of chlorine and bromine, Nature, 321, 759–762, 1986.

McLandress, C., Jonsson, A. I., Plummer, D. A., Reader, M. C., Scinocca, J. F., and Shepherd, T. G.: Separating the dynamical effects of climate change and ozone depletion. Part I: Southern Hemisphere stratosphere, J. Climate, 23, 5002–5020, doi:10.1175/2010JCLI3586.1, 2010.

Molina, L. T. and Molina, M. J.: Production of Cl_2O_2 from the self-reaction of the ClO radical, J. Phys. Chem., 91, 433–436, 1987.

Morgenstern, O., Braesicke, P., O'Connor, F. M., Bushell, A. C., Johnson, C. E., Osprey, S. M., and Pyle, J. A.: Evaluation of the new UKCA climate-composition model – Part 1: The stratosphere, Geosci. Model Dev., 2, 43–57, doi:10.5194/gmd-2-43-2009, 2009.

Morgenstern, O., Zeng, G., Abraham, N. L., Telford, P. J., Braesicke, P., Pyle, J. A., Hardiman, S. C., O'Connor, F. M., and Johnson, C. E.: Impacts of climate change, ozone recovery, and increasing methane on surface ozone and the tropospheric oxidizing capacity, J. Geophys. Res.-Atmos., 118, 1028–1041, doi:10.1029/2012JD018382, 2013.

The impact of polar stratospheric ozone loss

J. Keeble et al.

Orr, A., Bracegirdle, T. J., Hosking, J. S., Jung, T., Haigh, J. D., Phillips, T., and Feng, W. H.: Possible dynamical mechanisms for Southern Hemisphere climate change due to the ozone hole, J. Atmos. Sci., 69, 2917–2932, 2012a.

Orr, A., Bracegirdle, T. J., Hosking, J. S., Feng, W. H., Roscoe, H. K., and Haigh, J. D.: Strong dynamical modulation of the cooling of the polar stratosphere associated with the Antarctic ozone hole, J. Climate, 26, 662–668, doi:10.1175/JCLI-D-12-00480.1, 2012b.

Perlwitz, J., Pawson, S., Fogt, R. L., Nielsen, J. E., and Neff, W. D.: Impact of stratospheric ozone hole recovery on Antarctic climate, Geophys. Res. Lett., 35, L08714, doi:10.1029/2008GL033317, 2008.

Polvani, L. M., Waugh, D. W., Correa, G. J. P., and Son, S.- W.: Stratospheric ozone depletion: the main driver of 20th century atmospheric circulation changes in the Southern Hemisphere, J. Climate, 24, 795–812, doi:10.1175/2010JCLI3772.1, 2011.

Roscoe, H. K., Colwell, S. R., and Shanklin, J. D.: Stratospheric temperatures in Antarctic winter: does the 40-year record confirm midlatitude trends in stratospheric water vapour?, Q. J. Roy. Meteor. Soc., 129, 1745–1759. doi:10.1256/qj.02.173, 2003.

Schoeberl, M. R. and Hartmann, D. L.: The dynamics of the stratospheric polar vortex and its relation to the springtime ozone depletions, Science, 251, 46–52, 1991.

Schoeberl, M. R., Lait, L. R., Newman, P. A., and Rosenfield, J. E.: The structure of the polar vortex, J. Geophys. Res., 97, 7859–7882, doi:10.1029/91JD02168, 1992.

Shindell, D. T. and Schmidt, G. A.: Southern hemisphere climate response to ozone changes and greenhouse gas increases, Geophys. Res. Lett., 31, L18209, doi:10.1029/2004gl020724, 2004.

Sigmond, M. and Fyfe, J. C.: Has the ozone hole contributed to increased Antarctic sea ice extent?, Geophys. Res. Lett., 37, L18502, doi:10.1029/2010GL044301, 2010.

Sigmond, M., Reader, M. C., Fyfe, J. C., and Gillett, N. P.: Drivers of past and future Southern Ocean change: stratospheric ozone vs. greenhouse gas impacts, Geophys. Res. Lett., 38, L12601, doi:10.1029/2011GL047120, 2011.

Solomon, S.: Stratospheric ozone depletion: a review of concepts and history, Rev. Geophys., 37, 275–316, doi:10.1029/1999RG900008, 1999.

Solomon, S., Garcia, R. R., Rowland, F. S., and Wuebbles, D. J.: On the depletion of antarctic ozone, Nature, 321, 755–758, 1986.

Son, S.-W., Gerber, E. P., Perlwitz, J., Polvani, L. M., Gillett, N. P., Seo, K.-H., Eyring, V., Shepherd, T. G., Waugh, D., Akiyoshi, H., Austin, J., Baumgaertner, A., Bekki, S., Braesicke, P.,

The impact of polar stratospheric ozone loss

J. Keeble et al.

Bruhl, C., Butchart, N., Chipperfield, M. P., Cugnet, D., Dameris, M., Dhomse, S., Frith, S., Garny, H., Garcia, R., Hardiman, S. C., Jockel, P., Lamarque, J. F., Mancini, E., Marchand, M., Michou, M., Nakamura, T., Morgenstern, O., Pitari, G., Plummer, D. A., Pyle, J., Rozanov, E., Scinocca, J. F., Shibata, K., Smale, D., Teyssedre, H., Tian, W., and Yamashita, Y.: Impact of stratospheric ozone on Southern Hemisphere circulation change: a multimodel assessment, J. Geophys. Res., 115, D00M07, doi:10.1029/2010JD014271, 2010.

SPARC: SPARC Assessment of stratospheric aerosol properties (ASAP) SPARC Report No. 4, World Clim. Res. Programme, WCRP-124, WMO/TD-No. 1295, Berrieres le Buisson, Cedex, 2006.

Thompson, D. W. J. and Solomon, S.: Interpretation of recent Southern Hemisphere climate change, Science, 296, 895–899, 2002.

Thompson, D. W. J., Solomon, S., Kushner, P. J., England, M. H., Grise, K. M., and Karoly, D. J.: Signatures of the Antarctic ozone hole in Southern Hemisphere surface climate change, Nat. Geosci., 4, 741–749, doi:10.1038/ngeo1296, 2011.

Toon, O. B., Hammill, P., Turco, R. P., and Pinto, J.: Condensation of HNO_3 and HCl in the winter polar stratospheres, Geophys. Res. Lett., 13, 1284–1287, 1986.

Tuck, A. F.: Synoptic and chemical evolution of the Antarctic vortex in late winter and early spring, 1987, J. Geophys. Res., 94, 11687–11737, doi:10.1029/JD094iD09p11687, 1989.

Waugh, D. W., Randel, W. J., Pawson, S., Newman, P. A., and Nash, E. R.: Persistence of the lower stratospheric polar vortices, J. Geophys. Res., 104, 27191–27201, 1999

Waugh, D. W., Oman, L., Kawa, S. R., Stolarski, R. S., Pawson, S., Douglass, A. R., Newman, P. A., and Nielsen, J. E.: Impacts of climate change on stratospheric ozone recovery, Geophys. Res. Lett., 36, L03805, doi:10.1029/2008GL036223, 2009.

WMO: Scientific Assessment of Ozone Depletion: 2010, Global Ozone Research and Monitoring Project, Report No. 52, World Meteorological Organization, Geneva, Switzerland, 2011.

Young, P. J., Butler, A. H., Calvo, N., Haimberger, L., Kushner, P. J., Marsh, D. R., Randel, W. J., and Rosenlof, K. H.: Agreement in late twentieth century southern hemisphere stratospheric temperature trends in observations and CCMVal-2, CMIP3, and CMIP5 models, J. Geophys. Res., 118, 605–613, doi:10.1002/jgrd.50126, 2013.

The impact of polar stratospheric ozone loss

J. Keeble et al.
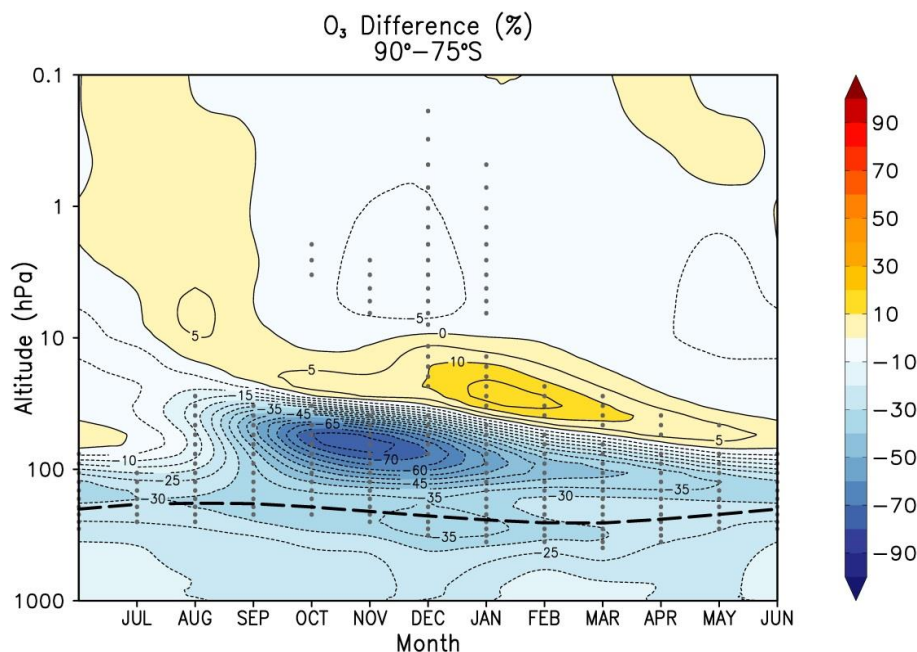
Figure 1. Zonal mean, monthly mean percentage ozone difference between REF2000 and NHC, averaged over 90–75° S. Contour intervals are 5 %, solid/dashed contours represent positive/negative changes. Stippling denotes significance at the 95 % confidence level. The bold dashed line signifies the tropopause height in the REF2000 simulation.
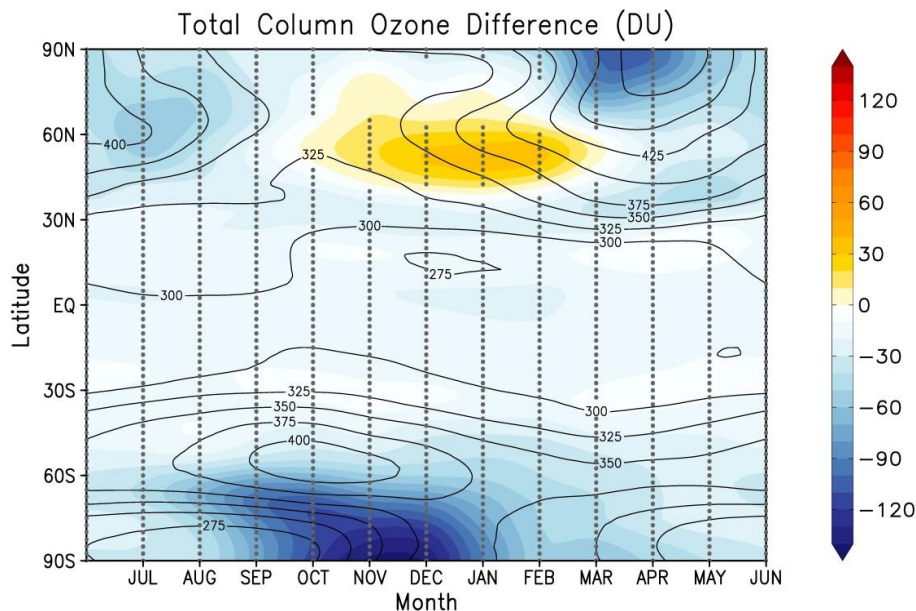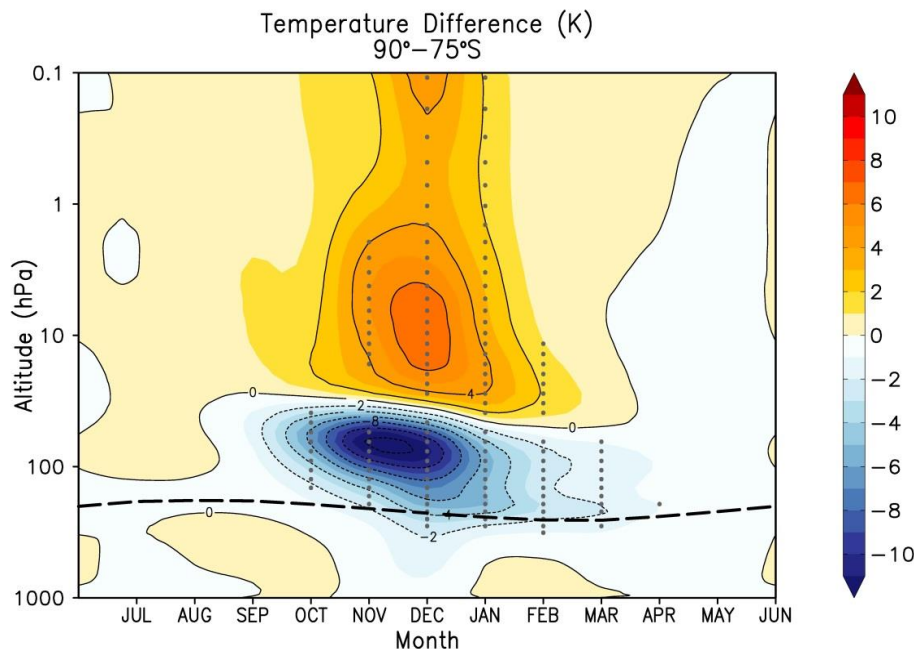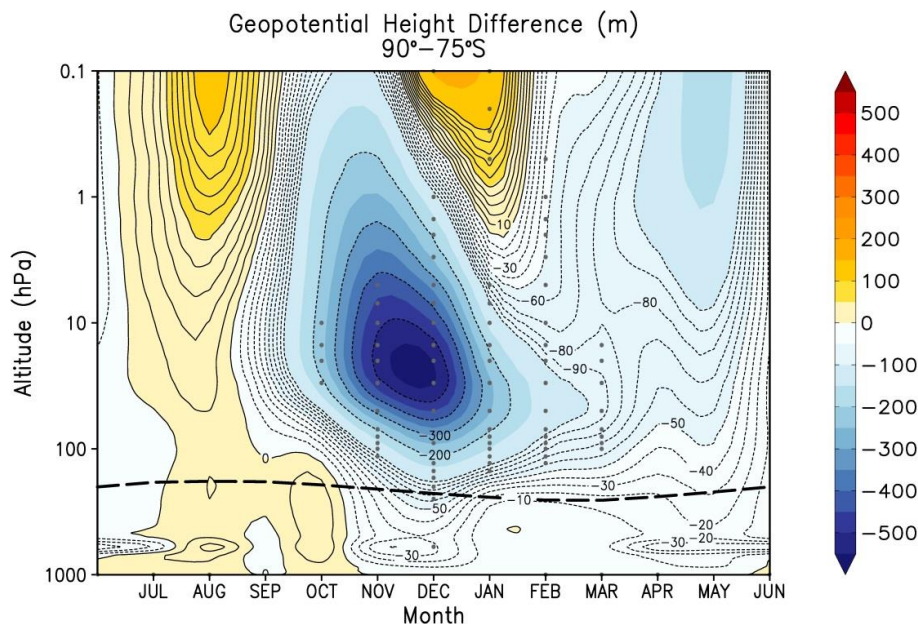
Figure 2. Zonal mean, monthly mean total column ozone REF2000 climatology (contours) and difference between REF2000 and NHC (shaded). Contour intervals are 25 Dobson Units, stippling denotes significance at the 95 % confidence level.

Figure 3. Zonal mean, monthly mean temperature difference between REF2000 and NHC, averaged over 90–75° S. Contour intervals are 2 K, solid/dashed contours represent positive/negative changes. Stippling denotes significance at the 95 % confidence level. The bold dashed line signifies the tropopause height in the REF2000 simulation.
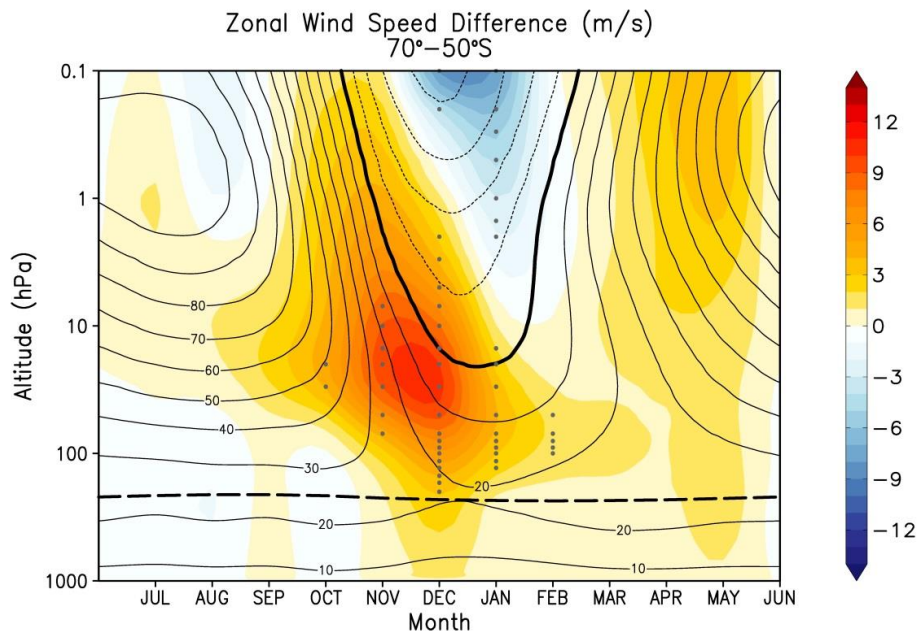
Figure 4. Zonal mean, monthly mean zonal wind REF2000 climatology (contours) and difference between REF2000 and NHC (shaded), averaged over 70–50° S. Contour intervals are $10\,\mathrm{m\,s^{-1}}$, solid/dashed contours represent positive/negative changes. $0\,\mathrm{m\,s^{-1}}$ contour is highlighted in bold. Stippling denotes significance at the 95 % confidence level. The bold dashed line signifies the tropopause height in the REF2000 simulation.

Figure 5. Zonal mean, monthly mean geopotential height difference between REF2000 and NHC, averaged over 90–75° S. Shaded contour intervals are 50 m, while contour lines are every 10 m from −100 to 100 m and every 100 m beyond this range. Solid/dashed contours represent positive/negative changes. Stippling denotes significance at the 95 % confidence level. The bold dashed line signifies the tropopause height in the REF2000 simulation.

Full Screen / Esc

Printer-friendly Version

Interactive Discussion
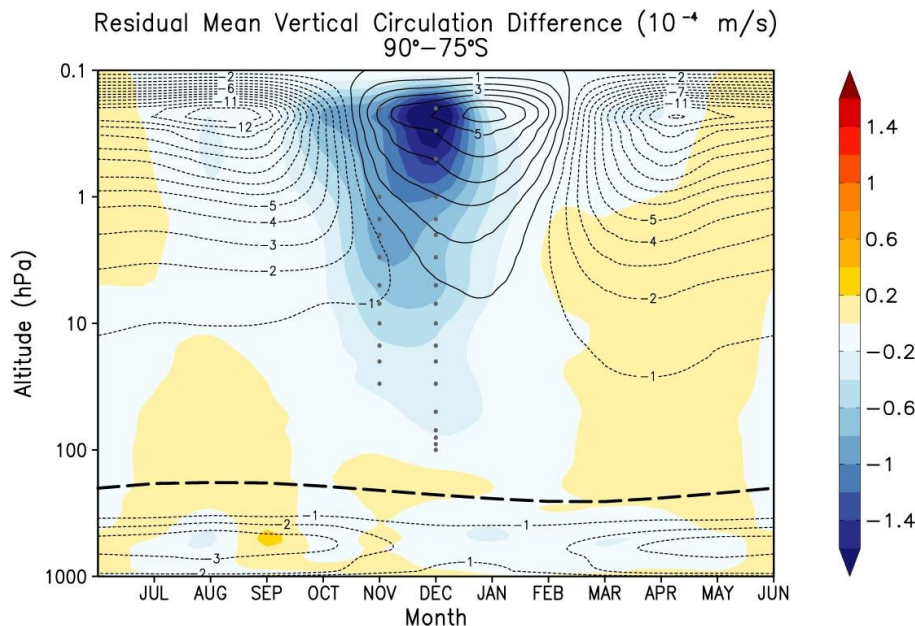
Figure 6. Zonal mean, monthly mean residual vertical velocity, $\overline{w}^*$, REF2000 climatology (contours) and difference between REF2000 and NHC (shaded) averaged over 90–75° S. Contour intervals are $1 \times 10^{-4}\,\mathrm{m\,s}^{-1}$, solid/dashed contours represent upwelling/downwelling respectively. Stippling denotes significance at the 95 % confidence level. The bold dashed line signifies the tropopause height in the REF2000 simulation.
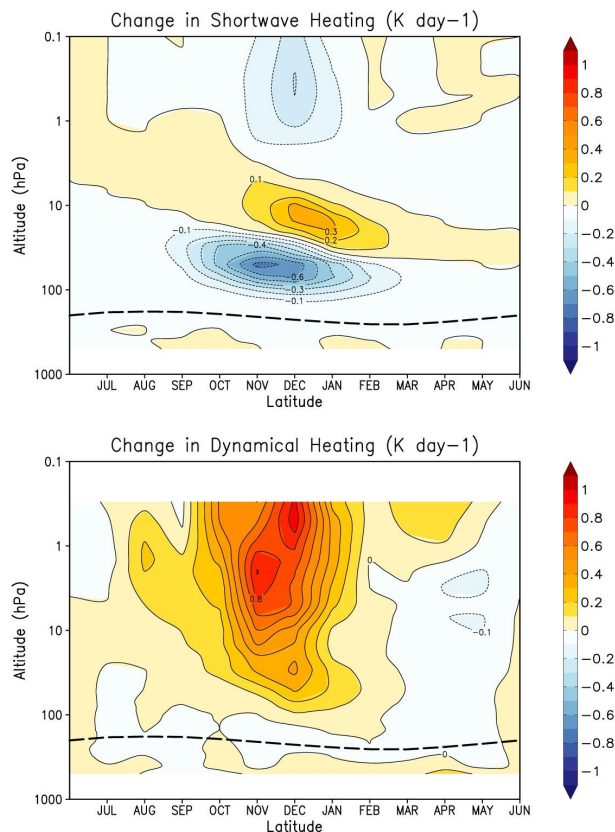
Figure 7. Zonal mean, monthly mean shortwave heating (top) and dynamical heating (bottom) differences between REF2000 and NHC, averaged over 90–75° S. Contour intervals are $0.1\,\mathrm{K\,day^{-1}}$. The bold dashed line signifies the tropopause height in the REF2000 simulation.
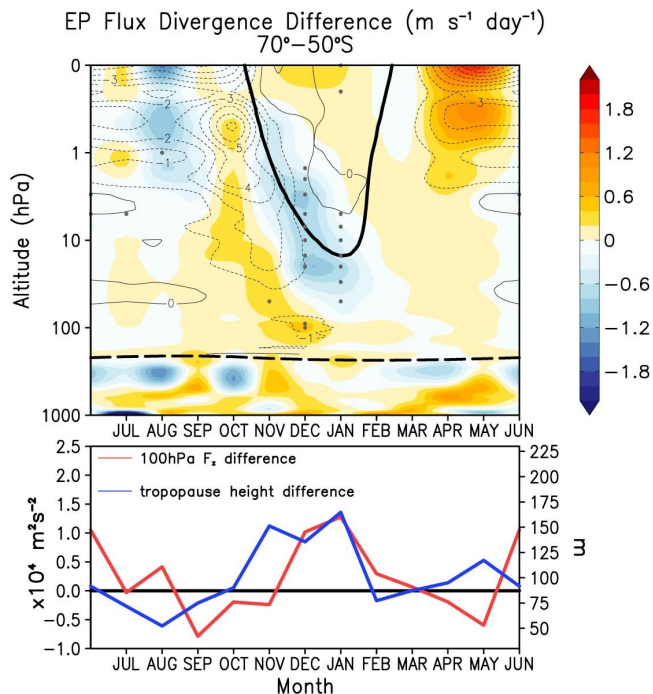
Figure 8. Zonal mean, monthly mean EP Flux divergence REF2000 climatology (contours) and difference between REF2000 and NHC (shaded), averaged over 70–50° S. Contour intervals are $1\,\mathrm{m\,s^{-1}\,day^{-1}}$, solid/dashed contours represent positive/negative changes. Stippling denotes significance at the 95 % confidence level. The zero wind line from REF2000 is highlighted in bold, while the bold dashed line signifies the tropopause height in the REF2000 simulation. The lower panel shows the zonal mean, monthly mean difference to the vertical component of the EP Flux, F_z ($\times 10^4\,\mathrm{m^2\,s^{-1}}$), in red (left hand axis), and the zonal mean, monthly mean difference to tropopause height (m) in blue (right hand axis), both averaged over 70–50° S.

Title Page

Abstract | Introduction

Conclusions | References

Tables | Figures

|◄ | ►|

◄ | ►

Back | Close

Full Screen / Esc
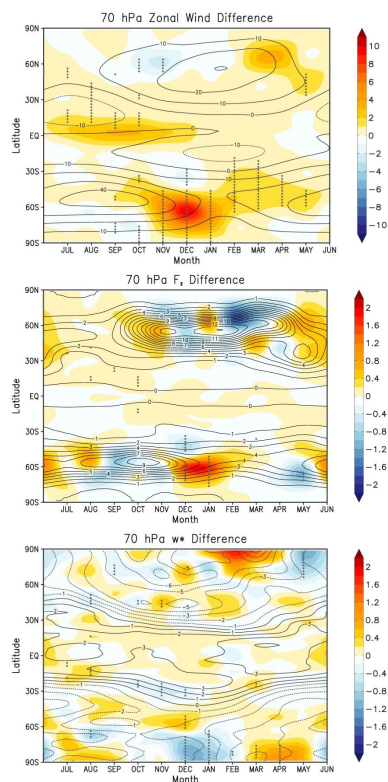
Printer-friendly Version

Interactive Discussion

Figure 9. Zonal mean, monthly mean, zonal wind (top); vertical component of the EP flux vector, F_z, (middle); and residual vertical velocity, $\overline{w}^*$, (bottom) REF2000 climatology (contours) and difference between REF2000 and NHC (shaded), at 70 hPa. Contour intervals for the REF2000 climatology are $10\,\mathrm{m\,s^{-1}}$ (top), $1 \times 10^4\,\mathrm{m^2\,s^{-2}}$ (middle) and $1 \times 10^{-4}\,\mathrm{m\,s^{-1}}$ (bottom). Stippling denotes significance at the 95 % confidence level.
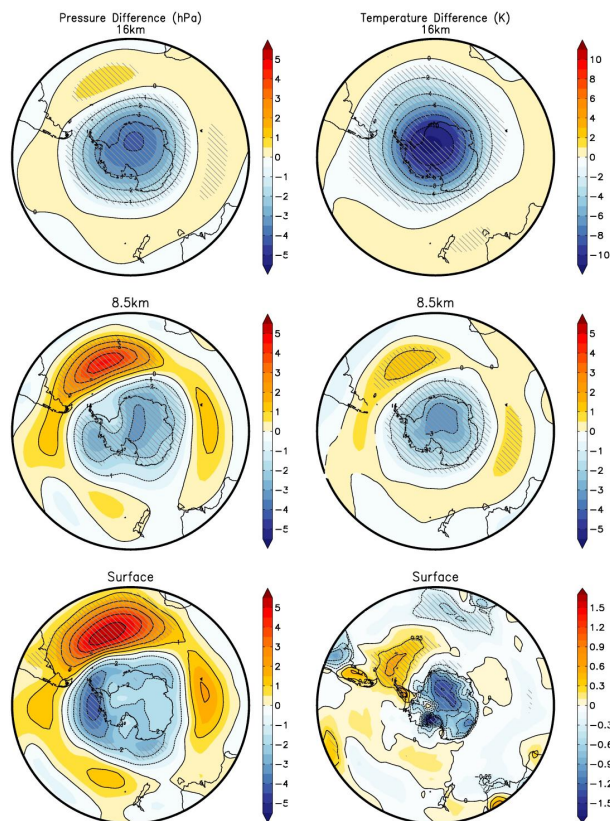
Figure 10. Stereographic plots of December pressure (left) and temperature (right) differences between REF2000 and NHC at 16 km (top), 8.5 km (middle) and the surface (bottom). Note the different scales for the temperature response at different altitudes. Hatching denotes significance at the 95 % confidence level.